Quantum Mechanical Threshold Resonances for Unsymmetric Potential Energy Barriers

ARTICLE *in* THE JOURNAL OF PHYSICAL CHEMISTRY · MARCH 1995

Impact Factor: 2.78 · DOI: 10.1021/j100010a032

3 AUTHORS, INCLUDING:

Ronald S Friedman
Indiana University-Purdue University Fort Wa…
43 PUBLICATIONS **1,045** CITATIONS
SEE PROFILE

Donald Truhlar
University of Minnesota Twin Cities
1,342 PUBLICATIONS **82,172** CITATIONS
SEE PROFILE

Reprinted from The Journal of Physical Chemistry, 1995, 99.

Quantum Mechanical Threshold Resonances for Unsymmetric Potential Energy Barriers

Ronald S. Friedman* and Vicki D. Hullinger†

Department of Chemistry, Indiana University Purdue University Fort Wayne, Fort Wayne, Indiana 46805-1499

Donald G. Truhlar

Department of Chemistry and Supercomputer Institute, University of Minnesota, Minneapolis, Minnesota 55455-0431

Received: August 16, 1994; In Final Form: November 29, 1994⊗

We consider quantum mechanical scattering by unsymmetric one-dimensional potential energy functions, and we locate poles of the scattering matrix in the complex energy plane for potential functions that exhibit two local maxima. For such cases, by using especially stable techniques for integrating the Schrödinger equation at complex energies, two quantum mechanical resonances are located, and the real parts of the resonance energies correlate well with the energies of the potential maxima. As the potential function is continuously transformed into one having a single maximum, the real parts of the two resonance energies approach each other, and the nearest pole to the real axis makes the dominant contribution to the observable collisional delay time. In the limit where a double barrier is transformed into a single barrier, the real parts of the two barrier poles become nearly equal, and the imaginary parts tend toward a ratio of about 3. These barrier resonances are further characterized by considering the relationship between the resonance width and the reactive delay time.

I. Introduction

The most widely used model for a chemical reaction is passage over a potential energy barrier. In a previous study[1] involving symmetric one-dimensional potential energy functions, we showed by direct numerical integration of the one-dimensional Schrödinger equation at complex energies subject to left-right scattering boundary conditions that metastable states associated with barriers are associated with poles of the scattering matrix (S matrix) just as are trapped states associated with standing waves in wells. Invoking the definition of a resonance as a pole of the scattering matrix,[2,3] we concluded that chemical reaction thresholds associated with barriers are quantum mechanical resonances. Although barrier resonances tend to be broader (and hence typically overlapped) and to be associated with shorter delay times than are conventional trapped-state resonances, we showed that there is no distinction in kind between the two kinds of poles of the S matrix in that passage over a barrier is associated with a pole of the scattering matrix that may be transformed continuously into a conventional resonance pole[2,3] by distorting the shape of the potential function. This previous study suggested that the study of chemical reactivity may be recast as a study of poles of the scattering matrix, and it provided support for multidimensional quantum dynamics calculations[4-6] of chemical reactions that associate transition-state threshold behavior with variational transition states.

The previous study[1] was concerned only with symmetric potential energy barrier functions, and the parameters of the potential were chosen to roughly resemble a one-dimensional model of the H + H_2 reaction. Most chemical reactions do not possess the high degree of symmetry considered in that earlier work, and multidimensional studies of the quantum dynamics of chemical reactions indicate that unsymmetric barriers lead to new resonance phenomena such as supernumerary transition states.[7] Thus, we were motivated to study unsymmetric one-dimensional potential functions to provide further insight into these resonance phenomena in the general case. In the present paper, we provide such a study with special emphasis on potentials with two unequal local potential barrier maxima. By varying the parameters in the potential energy function, we study the trajectories of resonances in the complex energy plane as the potential function is deformed from having two potential maxima to having only one potential maximum.

II. Theory

In this section we generalize the theoretical framework presented in ref 1. To discuss passage over a potential energy barrier, we consider the two-channel (left−right), one-dimensional scattering problem with boundary conditions in the two limits $x \to \pm\infty$. Channel 1 denotes the asymptotic region on the left ($x \to -\infty$), and channel 2 denotes that on the right ($x \to +\infty$). We solve the Schrödinger equation for scattering in one dimension x by a potential barrier function $V(x)$:

$$\frac{d^2\psi}{dx^2} + \frac{2\mu}{\hbar^2}[E - V(x)]\psi(x) = 0 \qquad (1)$$

where E is the energy and μ is the reduced mass. The potential $V(x)$ approaches $V_{+\infty}$ as $x \to \infty$ and approaches $V_{-\infty}$ as $x \to -\infty$. A particle with energy $E > \max[V_{+\infty}, V_{-\infty}]$ can be incident either from $x > 0$ or $x < 0$. Thus, the most general scattering boundary conditions are

$$\psi \underset{x\to-\infty}{\sim} \frac{N_-}{k_-^{1/2}}[C\exp(-ik_-x) + D\exp(ik_-x)] \qquad (2a)$$

$$\psi \underset{x\to+\infty}{\sim} \frac{N_+}{k_+^{1/2}}[A\exp(-ik_+x) + B\exp(ik_+x)] \qquad (2b)$$

where $N_\pm$ is an arbitrary normalization factor, and the asymptotic wavenumbers $k_\pm$ are given by

† Undergraduate research assistant.

⊗ Abstract published in *Advance ACS Abstracts,* February 15, 1995.

0022-3654/95/2099-3184$09.00/0

$$k_{\pm} = [2\mu(E - V_{\pm\infty})]^{1/2}/\hbar \tag{3}$$

(When E is real, we will always choose the positive root when computing wavenumbers. When E is in the fourth quadrant of the complex energy plane (with an argument between 0 and $-\pi/2$), then $k_{\pm}$ is also in the fourth quadrant (with an argument between 0 and $-\pi/4$).) The unitary scattering matrix (S matrix) relates the coefficients B and C of the outgoing waves to the coefficients A and D of the incoming waves:

$$\begin{pmatrix} C \\ B \end{pmatrix} = \begin{pmatrix} S_{11} & S_{12} \\ S_{21} & S_{22} \end{pmatrix} \begin{pmatrix} D \\ A \end{pmatrix} \tag{4}$$

Transmission and reflection coefficients can be computed from the scattering matrix elements.[8] In particular, reaction probabilities (transmission coefficients) P_{12} and P_{21} and reflection probabilities P_{11} and P_{22} are given by

$$P_{21} = |(C/A)|^2 = |S_{12}|^2 \tag{5a}$$

$$P_{22} = |(B/A)|^2 = |S_{22}|^2 \tag{5b}$$

$$P_{11} = |(C/D)|^2 = |S_{11}|^2 \tag{5c}$$

$$P_{12} = |(B/D)|^2 = |S_{21}|^2 \tag{5d}$$

The Schrödinger equation (1) can be solved at both real and complex energies E. Poles in the scattering matrix at complex energies

$$\bar{E} = E_R - i\Gamma/2 \tag{6}$$

correspond to resonances.[2,3] E_R is the real part of the resonance energy, and Γ is the resonance width, which is real and positive by definition. All the matrix elements S_{ij} have poles at $E = \bar{E}$ for each resonance energy $\bar{E}$. There are many methods in use for calculating complex resonance energies. In this paper, following Basilevsky and Ryaboy,[9] we search for poles of the S matrix by directly solving the Schrödinger equation at complex energies.

We may characterize a resonance in terms of a channel-to-channel delay time Δt_{ij}, which represents the time difference between a pulse being injected into channel i and a pulse appearing in channel j, relative to the same delay time in the absence of a potential $V(x)$.[10] The delay time is given in terms of the scattering matrix elements by[1,10]

$$\Delta t_{ij} = \mathrm{Im}\left(\hbar (S_{ji})^{-1} \frac{\mathrm{d}S_{ji}}{\mathrm{d}E}\right) \tag{7}$$

The scattered particle will experience a delay time at real energies E in the proximity of E_R. We expect the delay time to be large if the width Γ of the resonance is small.

III. Computational Methods

Locating and characterizing broad resonances (*i.e.*, those with large widths Γ) is a formidable task. In the present work, we used two different numerical techniques to look for poles of the S matrix far off the real energy axis. The first method, used previously,[1] was successful at locating the majority of resonances studied. However, this method had considerable difficulty locating very broad resonances. Therefore, we implemented a different numerical algorithm, which was much more successful at locating the broadest of resonances. We will describe each method in turn.

Before doing so, we restrict the present paper to potentials for which $V_{+\infty} = V_{-\infty} = 0$ and therefore $k_+ = k_- = k$. [But we do *not* assume $V(x) = V(-x)$.] For convenience we set $N_{\pm} = 1/k^{1/2}$. Furthermore, since $V(x)$ has a finite range, we assume that eq 2*a* holds to within acceptable numerical accuracy for $x \leq -a_1$, where a_1 is a positive number called the effective range in channel 1, and that eq 2*b* holds to within acceptable numerical accuracy for $x \geq a_2$, where a_2 is called the effective range in channel 2. The numerical values to be used for a_1 and a_2 depend on the accuracy sought, the width of the resonance, and other numerical parameters. In general, all numerical results must be converged with respect to increasing a_1 and a_2.

Since we consider complex E, the second-order differential equation (1) is also complex. In the first numerical method we transform it into four coupled real, first-order differential equations which we integrate directly. This method has been previously described in detail,[1] so we only summarize it here. We first consider a wave incident from $x > 0$ so we set $D = 0$; we normalize the solution so $C = 1$ in (2*a*). Thus we know the form of the solution of eq 1 as $x \to -\infty$; that is, we know the value of ψ and its first derivative ($\mathrm{d}\psi/\mathrm{d}x$) for $x \leq -a_1$. This solution is numerically propagated from $x = -a_1$ to $x = a_2$, at which point the coefficients A and B in (2*b*) are computed. The numerical propagation is carried out by a subroutine, DIVPAG, from the International Mathematical and Statistical Library (IMSL).[11] The library subroutine solves an initial value problem for ordinary differential equations using a variable step-size, Gear backward difference integrator[12] with a default maximum order of 5.

Scattering matrix elements are then obtained via

$$S_{22} = B/A \tag{8a}$$

and

$$S_{12} = 1/A \tag{8b}$$

To solve for the remaining two scattering matrix elements, we could have set $A = 0$ and $B = 1$ in eq 2*b* and subsequently propagated the solution from $x = a_2$ to $x = -a_1$, at which point the coefficients C and D in (2*a*) could be obtained. However, we used a simpler method to obtain S_{11} and S_{21}. It can easily be shown that if we follow the same procedure for determining S_{i2} by setting $D = 0$ and $C = 1$ but solve the Schrödinger equation (1) with the potential $V(-x)$, then the quantities computed by the ratios in (8*a*) and (8*b*) will be S_{11} and S_{21}, respectively. This is the method we used. We confirmed computationally that the scattering matrix is symmetric, *i.e.*, $S_{12} = S_{21}$. [In our previous work,[1] the potential $V(x)$ was an even function of x (symmetric), and $S_{11} = S_{22}$; that property does *not* hold here.]

Implementation of the Gear method required four numerical parameters which were varied until the scattering matrix elements were converged to better than 0.1%. These parameters were a tolerance parameter ϵ for control of the norm of the local error, an initial value Δx_1 of the stepsize, and the values of a_1 and a_2. The required values of the latter parameters were decreased by using the local wavenumber $[2\mu(E - V(x))]^{1/2}/\hbar$ rather than $k_{\pm}$ in the boundary conditions. For complex energies far off the real energy axis in the complex energy plane (Im $E < -2 \times 10^1$ meV), we found it increasingly difficult to converge the scattering matrix elements, and thus we sought another algorithm that would allow us to locate very broad resonances.

Before proceeding to describe the second algorithm used to locate resonances, it is instructive to consider why direct numerical integration of eq 1 does not yield satisfactorily converged results for scattering matrix elements for energies

far off the real energy axis. Let us denote the exact solution of eq 1 by ψ_{ex} and the exact boundary condition coefficients of eq 2*b* by A_{ex} and B_{ex}. Furthermore, denote the corresponding quantities obtained via numerical integration of eq 1 by ψ_{num}, A_{num}, and B_{num}. It is straightforward to show that the numerical error in A, that is, $A_{num} - A_{ex}$, is proportional to $\exp(ikx)(\psi_{num} - \psi_{ex})$, and likewise the numerical error in B, that is, $B_{num} - B_{ex}$, is proportional to $\exp(-ikx)(\psi_{num} - \psi_{ex})$, both for large, positive x. For energies in the fourth quadrant of the complex energy plane, the asymptotic wavenumber is also in the fourth quadrant; *i.e.*, k has a positive real part and a negative imaginary part. As a result, for positive x, $\exp(-ikx)$ is a product of an oscillating term and an exponentially decreasing term in x. However, $\exp(ikx)$ is a product of an oscillating term and an exponentially increasing term. Therefore, the numerical error in ψ is amplified when attempting to compute a converged value of A by increasing the value of x, *i.e.*, increasing a_2. Thus, although we encountered little difficulty in obtaining accurate values for B, we were not able to converge values of A, and as a result, our scattering matrix elements were not converged for complex energies far off the real energy axis.

The second method we used to obtain scattering matrix elements is based on the mathematical technique known as invariant imbedding.[13] Instead of solving the linear second-order eq 1 with the boundary conditions (2), an equivalent method[14] is to solve the following first-order, nonlinear initial value problem for the function $S(x)$:

$$\frac{dS}{dx} = 2ikS(x) + \frac{1}{2ik}U(x)[1 + S(x)]^2 \tag{9a}$$

$$S(-a_1) = 0 \tag{9b}$$

where $U(x) = 2\mu V(x)/\hbar^2$. The scattering matrix elements are then given by

$$S_{22} = S(a_2)\exp(-2ika_2) \tag{10a}$$

$$S_{12} = \exp\left(\frac{1}{2ik}\int_{-a_1}^{a_2} dx\, U(x)[1 + S(x)]\right) \tag{10b}$$

The first-order equation (9*a*) is decomposed into two real, first-order coupled differential equations as follows: Denoting

$$S(x) = S_r(x) + iS_i(x) \tag{11a}$$

$$k = (2\mu E)^{1/2}/\hbar = k_r + ik_i \tag{11b}$$

and

$$\varepsilon = \frac{1}{(2ik)} = \varepsilon_r + i\varepsilon_i, \tag{11c}$$

we have

$$dS_r/dx = S_r^2\varepsilon_r U(x) + S_r(-2k_i + 2\varepsilon_r U(x)) - S_i^2\varepsilon_r U(x) + S_i(-2k_r - 2\varepsilon_i U(x)) + S_r S_i(-2\varepsilon_i U(x)) + \varepsilon_r U(x) \tag{12a}$$

$$dS_i/dx = S_r^2\varepsilon_i U(x) + S_r(2k_r + 2\varepsilon_i U(x)) - S_i^2\varepsilon_i U(x) + S_i(-2k_i + 2\varepsilon_r U(x)) + S_r S_i(2\varepsilon_r U(x)) + \varepsilon_i U(x) \tag{12b}$$

At $x = -a_1$, the solution $S = (S_r, S_i) = (0,0)$. This solution is then numerically propagated to a large positive value $x = a_2$ using, as before, the IMSL subroutine DIVPAG. S_{22} is then computed by using eq 10*a*. To compute S_{12}, it is necessary to evaluate the integral in eq 10*b*. This is accomplished by using the Gear integrator to compute values of $S(x)$ at abscissas $x_j = -a_1 + jx_{inc}$ [the integer j runs from 0 to $(a_2 + a_1)/x_{inc}$] where x_{inc} is an input constant which is greater than or equal to Δx_1. The integral in eq 10*b* is then evaluated by using Simpson's rule.[15] The values of a_1, a_2, Δx_1, x_{inc}, and ϵ are varied until S_{22} and S_{12} are converged.

We determined poles in the S matrix (corresponding to resonances) by numerically searching for zeroes in $1/S_{ij}$. To find zeroes of $1/S_{ij}$ in the complex energy plane, we used a modified IMSL subroutine. The library subroutine, named ZANLY, invokes Muller's method[15] for quadratic interpolation among three points to find the next estimate of the root. The subroutine was modified to allow the user to input three initial guesses for the root (rather than providing only two guesses and letting the library subroutine itself determine the third initial guess). Muller's method of quadratic interpolation proved to be much more powerful than the secant method,[15] which uses linear interpolation between two points. The root-finding algorithm finished when the relative difference in two consecutive approximations to the root was within a parameter ERRREL, which we typically set to 10^{-10}.

Using the first method, direct numerical integration of eq 1, we successfully located poles of the S matrix at energies $\bar{E}$ for which Im $\bar{E} > -2 \times 10^1$ meV. For the narrower of the resonances located, we typically used $a_1 = 25a_0$, $a_2 = 25a_0$, $\epsilon = 10^{-10}$, and $\Delta x_1 = 10^{-3}a_0$; values of E_R and Γ calculated from S_{11}, S_{12}, S_{21}, and from S_{22} agreed to at least eight significant figures. For the broader of the resonances located, we found that $\bar{E}$ converged only if we decreased the range of numerical integration. Typical values were $a_1 = 10a_0$ and $a_2 = 10a_0$; the resonance energy parameters E_R and Γ calculated from the various S_{ij} elements agreed to at least five significant figures. For all of the resonances located by using the first method, E_R and Γ were converged with respect to the numerical integration parameters to at least four and sometimes up to nine significant figures.

Using the second method, invariant imbedding, we were able to locate the very broad resonances ($\Gamma/2 > 2 \times 10^1$ meV) as well as to check the results obtained by using the first method. To locate the poles of the S matrix which lie less than 2×10^1 meV off the real energy axis, we typically used $a_1 = 16a_0$, $a_2 = 14a_0$, $\epsilon = 10^{-9}$, and $\Delta x_1 = x_{inc} = 10^{-3}a_0$. The resonance energy parameters computed by using the two different methods agreed to at least five significant figures. To locate the very broad resonances ($\Gamma/2 > 2 \times 10^1$ meV), we found that we needed to drastically increase both a_1 and a_2, especially the final integration point a_2. For examples, for the resonance with $\Gamma/2 = 3.53 \times 10^1$ meV, we used $a_1 = 20a_0$, $a_2 = 30a_0$, $\Delta x_1 = x_{inc} = (5 \times 10^{-4})a_0$, and $\epsilon = 10^{-9}$; for the resonance with $\Gamma/2 = 3.88 \times 10^1$ meV, we used $a_1 = 20a_0$, $a_2 = 46a_0$, $\Delta x_1 = x_{inc} = (2.5 \times 10^{-4})a_0$, and $\epsilon = 10^{-10}$; and for the resonance with $\Gamma/2 = 4.15 \times 10^1$ meV, we used $a_1 = 32a_0$, $a_2 = 98a_0$, $\Delta x_1 = x_{inc} = (1 \times 10^{-4})a_0$, and $\epsilon = 10^{-10}$. We found that E_R and Γ calculated from S_{22} agreed with those calculated from S_{12} to three to five significant figures for these broad resonances and, furthermore, that E_R and Γ were converged with respect to the numerical integration parameters to at least three significant figures.

Reaction probabilities P_{21} and reflection coefficients P_{22} were computed at real scattering energies via direct numerical integration of eq 1 and the use of eqs 5*a* and 5*b*. To further bring out structure in the reaction probability as a function of energy, we computed the energy derivative of P_{21}. This was accomplished by fitting the reaction probabilities $P_{21}(E)$ in the energy range $(E_1, E_2, ..., E_M)$ to a cubic spline which is uniquely determined by requiring that the reaction probability and its first and second energy derivatives are continuous, that the cubic spline exactly reproduces all of the given reaction probabilities,

TABLE 1: Case Labels and Potential Characteristics

case	V_1, meV	β, a_0^{-1}	c	$V_{max}(1)$, meV	V_{min}, meV	$V_{max}(2)$, meV
A	598.64	3.00		166.95	145.74	166.95
B	653.06	3.00		180.37	-152.09	168.76
C	707.49	3.00		193.82	157.94	170.62
D	761.91	3.00		207.30	163.32	172.55
E	816.33	3.00		220.81	168.28	174.55
F	827.21	3.00		223.51	169.22	174.96
G	843.54	3.00		227.56	170.61	175.58
H	859.87	3.00		231.62	171.96	176.22
I	870.75	3.00		234.32	172.84	176.64
J	870.75	2.90		236.47	179.68	180.79
K	870.75	2.80		238.90		
L	870.75	2.60		244.72		
M	870.75	2.50		248.19		
N	870.75	2.40		252.09		
O	870.75	2.30		256.44		
P	870.75	2.25		258.79		
Q	870.75	2.20		261.27		
R	870.75	2.10		266.59		
S	870.75	2.00		272.38		
T	870.75	1.80		285.15		
U	870.75	1.70		291.92		
V			0.90	278.39		
W			0.80	265.11		
X			0.60	239.42		
Y			0.40	214.69	200.99	202.27
Z			0.20	190.61	173.70	183.64

and that the first derivatives of P_{21} at E_1 and E_M are zero. (The latter condition was ensured by choosing a sufficiently large energy range.)

Delay times Δt_{ij} defined in eq 7 were also obtained at real scattering energies as previously described.[1,16] The scattering matrix elements were fit at three consecutive real energies to the form

$$S_{ji}(E) = (c_1 + c_2E + c_3E^2)\exp[i(c_4 + c_5E + c_6E^2)] \quad (13)$$

where c_n are real fitting parameters. Then the delay time was obtained at the central energy of the triad by

$$\Delta t_{ij}(E) = \hbar(c_5 + 2c_6E) \quad (14)$$

Note that a factor of 2 is missing in eq 15 of ref 1.

IV. Calculations

For the present study, we considered potentials of the form

$$V(x) = \frac{V_1 e^{\beta_1(x-x_1)}}{(1+e^{\beta_1(x-x_1)})^2} + \frac{V_2 e^{\beta_2(x-x_2)}}{(1+e^{\beta_2(x-x_2)})^2} \quad (15)$$

and used the reduced mass $\mu = 6526.3m_e$. Potential parameters were chosen to roughly represent a one-dimensional model of the O + D_2 reaction; in particular, with $V_1 = 870.75$ meV, $V_2 = 598.64$ meV, $\beta_1 = \beta_2 = 3a_0^{-1}$, and $x_2 = -x_1 = 0.6a_0$, the potential very roughly resembles the $v_1 = 1$ vibrationally adiabatic potential of the aforementioned reaction.[17]

In general, we will denote the energy of the global potential barrier maximum as $V_{max}(1)$ or simply V_{max}. If the potential has a second local potential maximum, it will be denoted $V_{max}(2)$, and the local minimum between the two maxima will be denoted V_{min}.

Two series of potential functions, all having the general form of eq 15, were used in our study. In series I, we were particularly interested in unsymmetric potential functions which had two potential barrier maxima. In this series, we took $V_2 = 598.64$ meV, $\beta_1 = \beta_2 = \beta = 3a_0^{-1}$, $x_2 = -x_1 = 0.6a_0$, and V_1 was variable. Nine different values of V_1 were considered and labeled cases A–I as shown in Table 1. Figures 1 and 2 show potential energy functions for representative cases in series I. As seen, potentials B–I are unsymmetric and have two maxima, with the lower local barrier maximum becoming less prominent as we proceed from case B to case I.

In series II, we considered potential functions that are continuously deformed so that eventually only one potential barrier maximum appears, rather than two. For this series, we took $V_1 = 870.75$ meV, $V_2 = 598.64$ meV, $x_2 = -x_1 = 0.6a_0$, and $\beta_1 = \beta_2 = \beta$ was variable. Thirteen different values of β were considered and labeled cases I–U as shown in Table 1. Note that the last member of series I is identical to the first member of series II. Figures 3–5 show $V(x)$ for representative cases; as seen, K–U have only one, rather than two, barrier maximum.

Reaction probabilities $P_{21}(E)$ and their derivatives dP_{21}/dE, as well as reactive delay times $\Delta t_{21}(E)$, were computed, and selected results are presented in Figures 1–5.

Poles of the S matrix were also located for all cases; in each case, two resonances were found. Values of E_R are indicated by horizontal lines in the plots of the potential functions in Figures 1–5 and by vertical lines in the remainder of the plots in Figures 1–5. The width Γ is also indicated for each resonance next to the horizontal lines in Figures 1–5.

The poles of the scattering matrix for these 21 cases are shown in the complex energy plane in Figure 6. Additional calculations were also carried out for five potentials of the form

$$V(x) = cV^U(x) + (1-c)V^A(x) \quad (16)$$

where $V^A(x)$ and $V^U(x)$ are the potential functions of cases A and U, respectively, and $c = 0.2$, 0.4, 0.6, 0.8, and 0.9. These latter five potential functions smoothly connect one $V(x)$ from series I (case A) to one $V(x)$ from series II (case U). This will be called series III. Poles resulting from the additional calculations are also shown in Figure 6. The pole positions are connected by a curve which shows their 'trajectory' through the complex energy plane as a function of the potential parameters.

Table 1 shows the labels and potential characteristics for the 26 cases A–Z. For each potential, we refer to the resonance with the smaller (larger) value of E_R as the lower (higher) energy resonance. Table 2 shows characteristics of the resonance energy parameters of each case for the higher energy resonance [$E_R(1)$, $\Gamma(1)$] and the lower energy resonance [$E_R(2)$, $\Gamma(2)$].

For many of the reactive delay time curves in Figures 1–5, there are two peaks. In such cases, there is very good agreement between the energies of the local maxima of $\Delta t_{21}(E)$ and the values of E_R of the two resonances for that particular potential. As a consequence, we can associate each delay time peak with a resonance. Figure 7 is a plot of the value of the local maximum in $\Delta t_{21}(E)$ versus the inverse of the width ($1/\Gamma$) of the associated resonance. We have also included in this figure results from the calculations of ref 1. Cases labeled a–c correspond to the first three cases in that study; in each case, one resonance was located and one peak in the reactive delay time was observed. Cases labeled e–h correspond to the last four cases in that study; in each case, two peaks in Δt_{21} were observed and two poles were located.

V. Discussion of Results

We will consider the various cases in order and, in particular, focus on the relationship between the real part, E_R, of the resonance energy and the energy, $V_{max}(1)$ or $V_{max}(2)$, of the potential maximum and on the relationship between the resonance width Γ and the reactive delay time Δt_{21} at real energies in the vicinity of E_R.

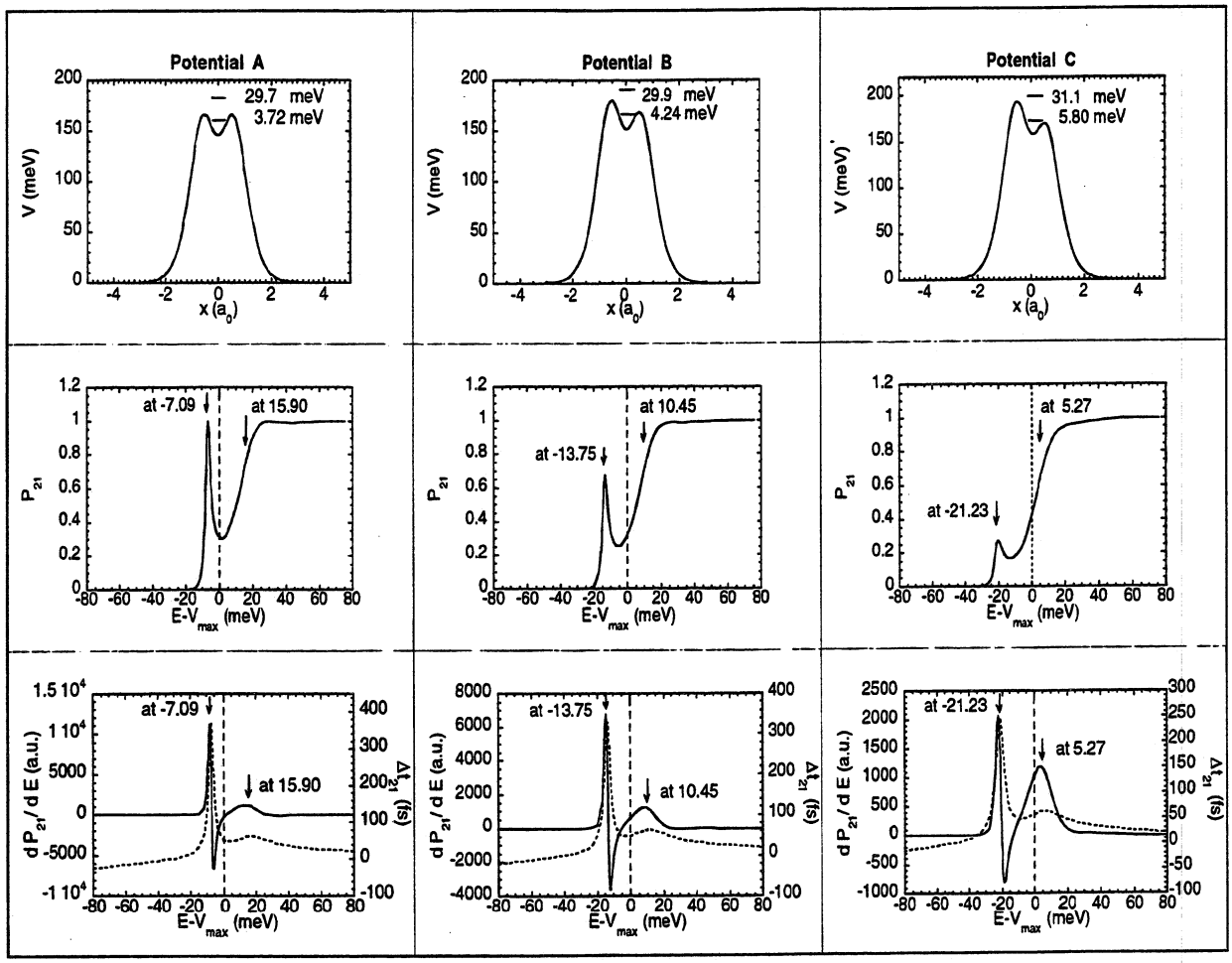

Figure 1. Results for cases labeled A, B, and C. Top: Potential shapes. Horizontal lines indicate E_R, the real part of the resonance energy, and the numbers next to the horizontal lines report Γ, the resonance width, in meV. Middle: Reaction probabilities. Bottom: Derivatives of the reaction probabilities (solid curves with scale at left) and reactive delay times (dashed curves with scale at right). In the middle and bottom, the vertical arrows indicate E_R at the reported values of $E_R - V_{max}$, and a dashed vertical line is drawn at $E = V_{max}$.

V.A. Series I. We begin with the potentials of series I. Case A is a symmetric potential and, as shown in Figures 1 and 6, two poles of the S matrix were located. The narrower resonance has a value of E_R that is 7.09 meV below $V_{max}(1) = V_{max}(2)$; thus this corresponds to a subthreshold trapped state. The broader resonance has a value of E_R that is 15.90 meV above $V_{max}(1)$ and thus is a suprathreshold resonance. The broader resonance is presumably associated with the potential well even though its energy exceeds the energy required classically to escape the well. (The fact that a well resonance can occur at an energy above that required classically to escape is well-known.[1,8]) The reaction probability in Figure 1 rises from 0 toward 1 and then begins to decrease before rising toward unity again. The two rises in P_{21} coincide with peaks in both dP_{21}/dE and Δt_{21} as also seen in Figure 1. The structure shown in the three curves also corresponds very well to the real parts of the two resonance energies (see the vertical lines in Figure 1). Furthermore, the maximum delay time of 372 fs associated with the narrower resonance exceeds the maximum Δt_{21} of 63 fs associated with the broader resonance.

The potential for case B is unsymmetric and has two potential barrier maxima. As for case A above, there is a broader resonance above $V_{max}(1)$, associated with the rise in P_{21} toward unity and peaks in the derivative and reactive delay time curves. There is also a narrower resonance below $V_{max}(2)$, barely trapped in the potential well, with which is also associated peaks in dP_{21}/dE and Δt_{21}. Again, as expected, the maximum in the delay time is larger for the narrower of the peaks. However, the reaction probability only rises to 0.67 in the vicinity of the lower energy resonance. Compared to the lower energy resonance of case A, this resonance in case B is broader, and its effect on the reaction probability is diminished. Small rises (to significantly less than 1) in the reaction probability have also been observed in other model studies of unsymmetric potentials.[18,19]

For the potential of case C, the lower energy resonance now lies slightly above the energy of the potential well [*i.e.*, the energy of the smaller potential barrier maximum $V_{max}(2)$] and is associated with the rise in P_{21} to only 0.27. As we proceed from case A to case I, the lower-energy resonance is getting progressively broader (see Figure 6) and is associated with smaller rises in the reaction probability and smaller maxima in the reactive delay time. The real part of the resonance energy lies in the vicinity of the lower potential barrier maximum; *i.e.*, near $V_{max}(2)$ (see Figures 1 and 2). The derivative dP_{21}/dE enhances the structure in the reaction probability; for example, compare the plots of P_{21} and dP_{21}/dE for case I in Figure 2. Figure 7 clearly shows that the maximum delay time is inversely proportional to the width of the associated lower energy resonance.

The higher energy resonance for the potential of case C lies 5.27 meV above $V_{max}(1)$. As we proceed from case A to case I, we see from Figure 6 that the higher energy resonance moves progressively lower in energy relative to $V_{max}(1)$ and also gets progressively broader. However, in relative terms, the progressive increase in width is not as rapid for the higher energy resonance as for the lower energy resonance. For example, for the higher energy resonance, Γ has increased by a factor of 1.5

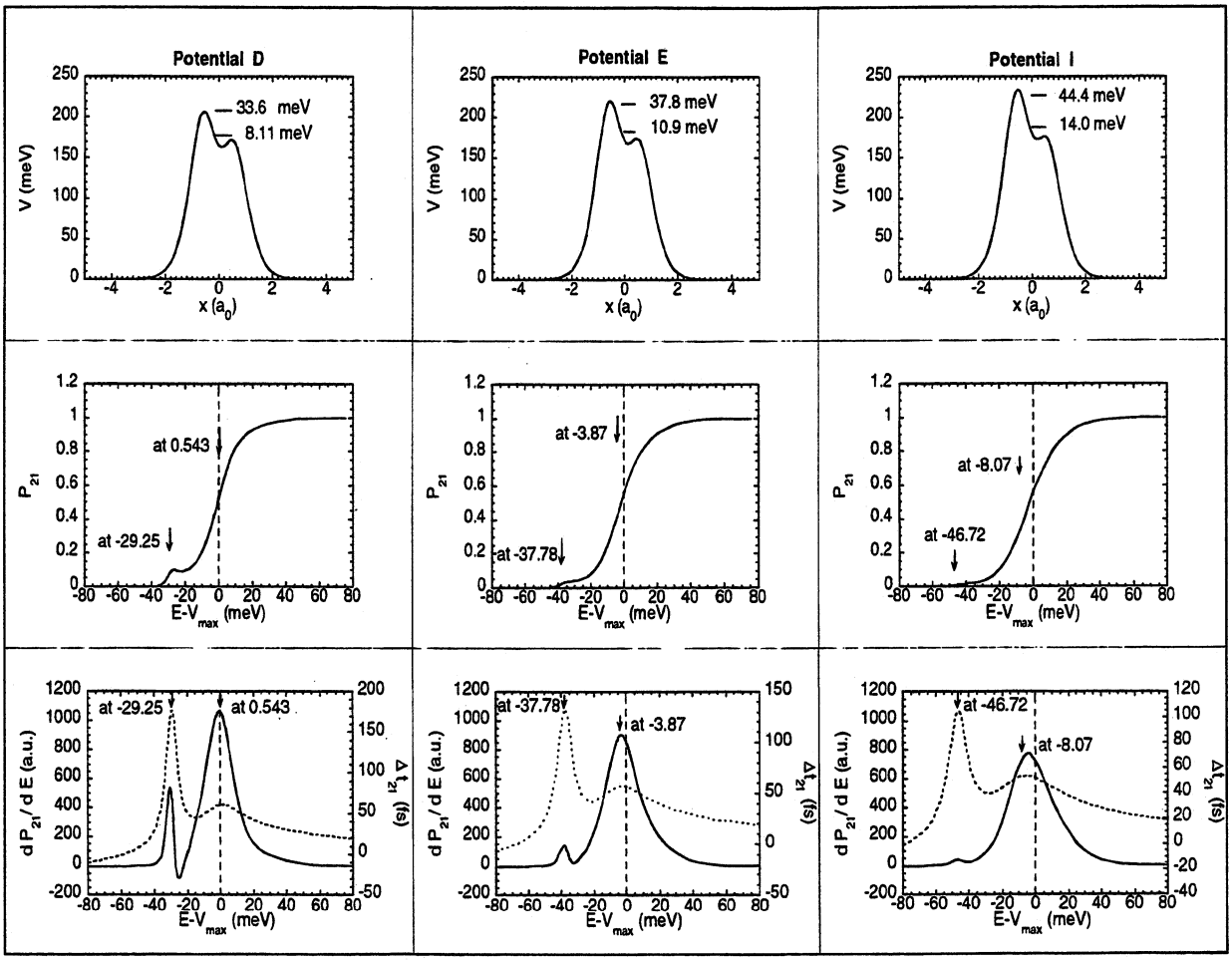

Figure 2. Same as Figure 1 except for cases D, E, and I.

from case A to case I, while, for the lower energy resonance, Γ increases by a factor of 3.8. Associated with the higher energy resonance is a rise in the reaction probability toward unity and peaks in dP_{21}/dE and Δt_{21}. Figure 7 (see insert) demonstrates again the inverse relationship between the resonance width and the maximum in the delay time.

Several important conclusions can be drawn from the study of potentials in series I. For each potential, two poles of the S matrix were determined, and, in general, each resonance lies in the vicinity of a local potential barrier maximum. The higher energy resonance, which is always broader, is associated with a rise toward 1 in the reaction probability and with peaks in both the derivative and delay time curves. As the resonance moves lower in energy relative to $V_{max}(1)$, it gets broader in width and is associated with a smaller delay time. The lower energy resonance lies in the vicinity of the smaller potential barrier maximum, and as we begin to transform the potential function toward one having only a single barrier maximum, the lower energy resonance gets progressively broader, its effect on the reaction probability is increasingly diminished, and its peak in the delay time gets smaller. The derivative curves become more useful in elucidating the effect of the lower energy resonance on the reaction probability as the resonance gets broader.

V.B. Series II. We next consider the potentials of series II. For the potential of case I (the case which occurs in both series I and II), two resonances are located, both lying below $V_{max}(1)$ and separated by 38.65 meV. The higher energy resonance, with which is associated the rise in P_{21} toward 1, is a factor of 3.2 times broader than the lower energy resonance, whose E_R value is 10.96 meV above the lower potential maximum. The effect of the lower energy resonance on the reaction probability appears to be very small. Being the narrower of the two resonances, the lower energy resonance is associated with a larger peak in the delay time in the vicinity of E_R.

For the potential of case J, the local potential maximum at low energies is less pronounced than in case I. Compared to I, the two resonances in J have moved higher in energy relative to $V_{max}(1)$ (see Figure 6), but, while the width of the higher energy resonance has changed very little (44.5 meV for case J compared to 44.4 meV for case I), the width of the lower energy resonance has increased by a factor of 1.2. The two resonances of case J are separated by 37.44 meV. Two peaks in Δt_{21} appear, the larger peak associated with the narrower resonance at lower energy. As we proceed to case K, the local potential maximum at lower energy now appears as a shoulder. Both resonances move higher in energy relative to $V_{max}(1)$, and now they are separated by 35.62 meV. Compared to case J, the higher energy resonance has gotten very slightly narrower, while the lower energy resonance is significantly broader; the ratio of the width of the higher energy resonance to that of the lower energy resonance for case K is 2.1. The effect of the lower energy resonance on P_{21} is barely noticeable in the derivative curve of Figure 3. There are still two peaks in the reactive delay time but they are beginning to overlap more as the values of E_R of the two resonances approach. The inverse relationship between the peak in Δt_{21} and Γ is clearly observable in Figure 7 for the narrower resonances of cases I–K.

As we proceed from cases I to T, as seen in Figures 2–5, the second potential maximum becomes a shoulder in $V(x)$ and then disappears, leaving only one potential barrier maximum.

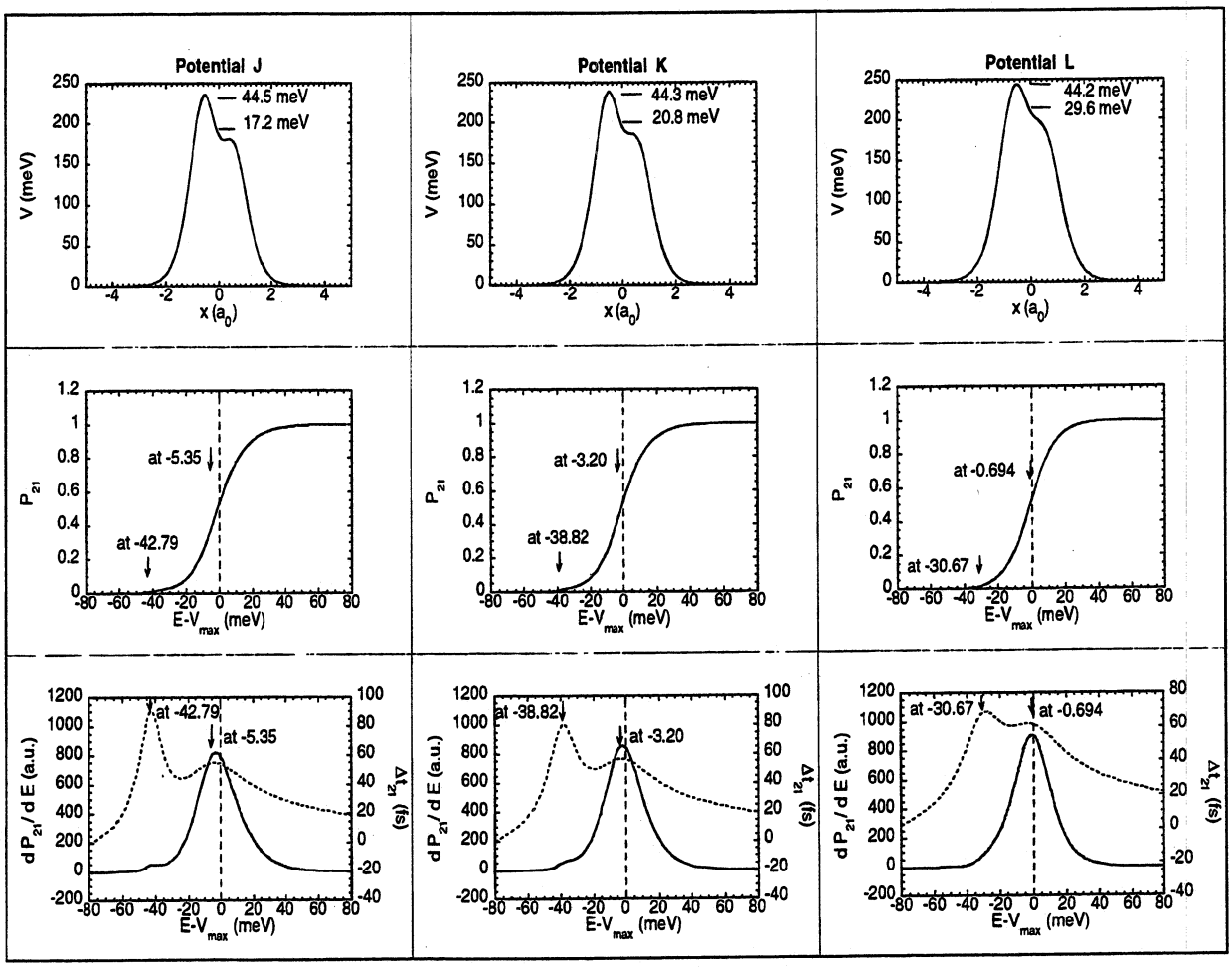

Figure 3. Same as Figure 1 except for cases J, K, and L.

However, two poles of the S matrix are still located. The values of E_R of the two resonances get closer and closer, and, while the width of the higher energy resonance *decreases*, that of the lower energy resonance *increases* dramatically (see Figure 6). In case T, the lower energy resonance is now nearly a factor of 3 times *wider* than the higher energy resonance. Table 2 demonstrates the variations of the difference in E_R and of the ratio of Γ for the two resonances with the potential function parameter β (specified in Table 1) of series II.

Furthermore, still considering the progression from case I to case T, we see that the two peaks in the reactive delay time curves overlap more and more until they merge into a single peak. This is consistent with the values of E_R of the two resonances of each potential getting closer. As seen in Figure 7, when two peaks are observed, there is an inverse relationship between the maximum in Δt_{21} and the width Γ of the resonance whose E_R lies closest to the energy of the delay time peak. Cases N–T, for which only one peak in Δt_{21} was observed, are not depicted in Figure 7. However, even in these latter cases, there is an inverse relationship between the maximum in the delay time and the width of the *higher* energy resonance. This is clearly demonstrated in Table 3 for cases N, O, Q, S, and T. (Time delays were not computed for cases P and R.) The table shows that as the two resonances for each case get closer in their values of E_R, there is an excellent correlation between E_R of the higher energy resonance and the energy E_{max} at which there is a maximum in the delay time. Furthermore, the decrease in the width of the higher energy resonance parallels the increase in the maximum delay time. In contrast, the width of the lower energy resonance *increases*. Thus, the higher energy resonance (which is becoming much narrower than the lower energy resonance) makes the dominant contribution to the reactive delay time.

To complete the analysis of series II, as we proceed from case T to case U, the lower energy resonance gets slightly narrower (see Figure 6). From Table 2, we see that the ratio of the lower energy resonance width to the higher energy resonance width drops slightly, and the E_R values of the two resonances also move slightly further apart. As above, the higher energy resonance appears to make the dominant contribution to the reactive delay time as seen in Table 3 by the 0.06-meV difference between E_R of the higher energy resonance and the energy of the maximum in the delay time.

V.C. Series III. Five additional potentials were considered—of the form of eq 16. Figure 6 shows how their resonance energies vary in the complex energy plane with the potential parameter c.

V.D. General Discussion. The observed variation of the ratio of resonance widths with the potential function agrees nicely with previous analytical and numerical studies of model one-dimensional barriers. Atabek *et al.*[20] analytically solved the Schrödinger equation for a harmonic barrier (*i.e.*, an inverted parabola) and found a series of poles of the S matrix accumulating at an energy corresponding to the top of the potential barrier. Furthermore, the width of the resonances (each resonance characterized by an integer $n = 0, 1, 2, ...$) varied as $2n + 1$. A treatment of the harmonic barrier by Seideman and Miller[21] yielded an identical result for the poles of the S matrix (Siegert eigenvalues). Thus, we expect that for the parabolic barrier, the ratio of the widths of the two narrowest resonances ($n = 0$, 1) is exactly 3. In fact, this also follows from a naive analytic

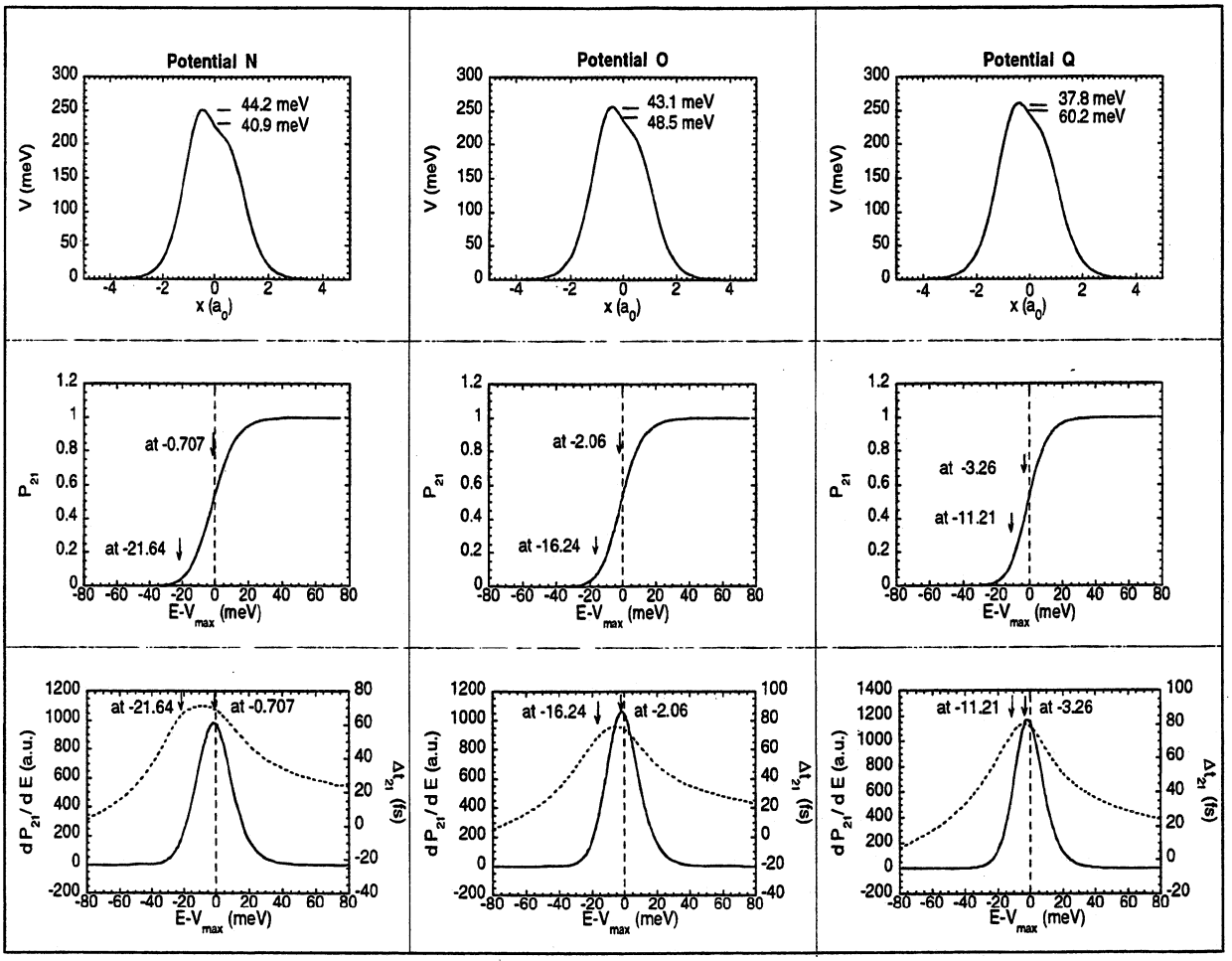

Figure 4. Same as Figure 1 except for cases N, O, and Q.

continuation of the results for a harmonic oscillator. For

$$V(x) = V_0 + \frac{1}{2}\mu\omega^2 x^2 \tag{17}$$

the eigenvalues, which are poles of the S matrix, are $V_0 + {}^1/_2\hbar\omega \cdot (v + {}^1/_2)$, $v = 0, 1, \ldots$ Letting ω^2 become negative, which transforms $V(x)$ from a harmonic oscillator to a parabolic barrier, yields poles at $V_0 - {}^1/_2\hbar|\omega|i(v + {}^1/_2)$, $v = 0, 1, \ldots$; *i.e.*, the widths of the first two resonances are in a ratio of 3. Analytical and numerical treatments of symmetric Eckart potentials by Ryaboy and Moiseyev[22] using the complex coordinate method also yielded a series of complex Siegert eigenvalues labeled by a nonnegative integer n whose widths Γ varied as $(n + {}^1/_2)$. (It should be noted that the latter authors also considered analytical and numerical treatments of nonsymmetric Eckart potentials. However, the nonsymmetric potentials of ref 22 differ from those studied here; in ref 22, the nonsymmetric potentials possess one potential maximum but are asymmetric in their asymptotic energies. That is, $V_{+\infty} \neq V_{-\infty}$.)

When two peaks are apparent in the delay time, there is an excellent correlation between the energy at which Δt_{21} is a maximum and the value of E_R. See, for example, cases A–L in Figures 1–3. As observed in Figures 1–5, there is also a strong correlation between E_R and the energy at which a peak (or shoulder) in dP_{21}/dE occurs.

In cases A–I, both the lower and higher energy resonances appear to contribute to separate features in the transmission probability P_{21}. (See Figures 1 and 2.) In case I, the contribution from the lower energy resonance appears to be a plateau in P_{21}. As the lower energy resonance gets broader as we proceed from case I to case T, its contribution to P_{21} appears to get smaller until there is one continuous rise in the reaction probability from 0 toward 1 and only one observable peak in the derivative plot. A question arises as to whether the broader lower energy resonance makes *any* contribution to the reaction probability in, for example, cases S and T. Ryaboy and Moiseyev[22] proved that the (cumulative) reaction probability for an Eckart potential can be expressed in terms of all the Siegert poles of the scattering matrix, even though the energy dependence of P_{21} is structureless. Similarly, Seideman and Miller[21] showed how the reaction probability can be expressed in terms of Siegert eigenvalues (using flux correlation functions) for parabolic and Eckart barriers. It is interesting that the authors[21,22] do not regard the reaction probability in such a case as demonstrating resonance behavior. We suggest that, although from one point of view such questions involve arbitrary semantic distinctions, from another point of view the extension of the resonance language to threshold phenomena has several practical and conceptual advantages.[1] First, it provides a unification of various related phenomena, since, as demonstrated both in ref 1 and here, trapped-state resonances transform continuously into threshold resonances and vice versa. Thus there can be no fundamental distinction between the two types of poles of the S matrix. Second, treating threshold poles as resonances provides a new perspective on variational transition-state theory, which leads to new computational approaches for practical problems, such as the calculation of anharmonic quantized transition-state energy levels in variational transition-state theory[23] or the calculation of delay times for passing through dynamical bottlenecks.[5]

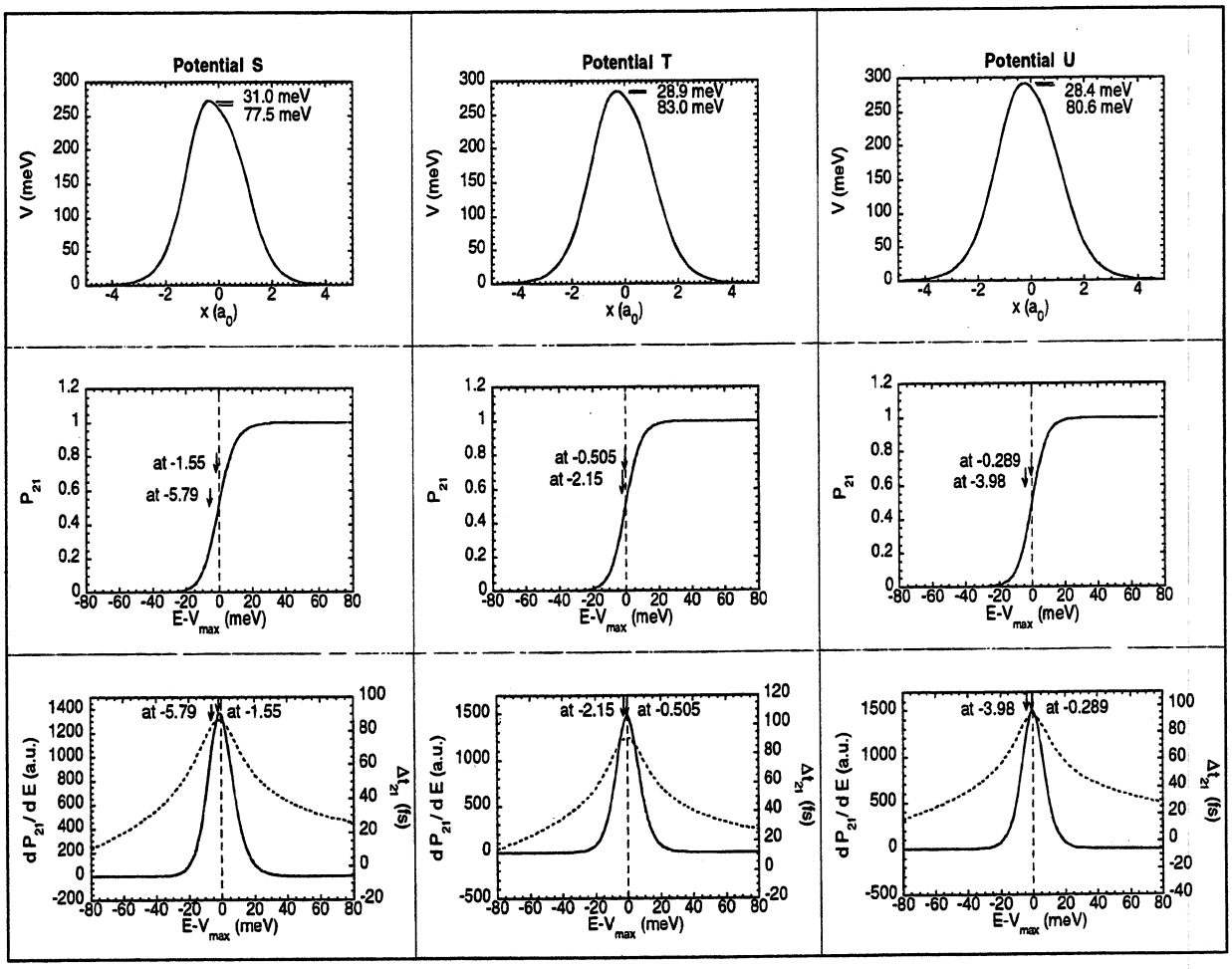

Figure 5. Same as Figure 1 except for cases S, T, and U.

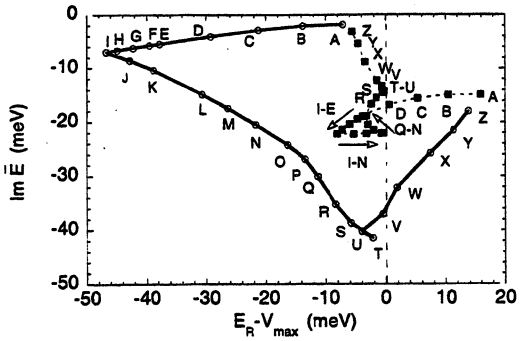

Figure 6. Trajectory of resonance poles. A dashed vertical line is drawn at $E_R - V_{max} = 0$. The calculations are labeled by the case label of Table 1. The solid and dashed lines smoothly connect one of the two resonances for each case with one of the two resonances for a subsequent case.

This latter point is strongly reinforced by the present results. Thus, even when the poles begin to "line up" in the pattern characteristic of a parabolic barrier [*i.e.*, $E_R(2) \approx E_R(1)$ and $\Gamma(2) \approx 3\Gamma(1)$], the dominant contribution to the physically observable delay time is made by the narrower resonance, *i.e.*, the resonance with parameters $E_R(1)$ and $\Gamma(1)$. (See, for example, the discussion of cases N–T in Section *V.B.*) Thus, although the resonances in this case are broad and overlapping, the nearest pole to the real axis is useful for understanding the dynamics in real time, an issue of increasing importance in light of recent advances in femtosecond spectroscopy.[24] Of course, none of these conclusions contradict the well-known fact that the simple isolated narrow-resonance formulas[3,5] should not be invoked without caution for the case of broad, overlapping resonances.

TABLE 2: Characteristics of the Resonance Energy Parameters E_R and Γ for the Higher Energy Resonance [$E_R(1),\Gamma(1)$] and Lower Energy Resonance [$E_R(2),\Gamma(2)$]

case	$E_R(1) - E_R(2)$, meV	$E_R(1) - V_{max}(1)$, meV	$E_R(2) - V_{max}(2)$, meV	$\Gamma(2)/\Gamma(1)$
A	22.99	15.90	−7.09	0.125
B	24.20	10.45	−2.14	0.142
C	26.50	5.27	1.97	0.186
D	29.79	0.54	5.50	0.241
E	33.91	−3.87	8.48	0.288
F	34.81	−4.73	9.01	0.296
G	36.22	−5.99	9.77	0.305
H	37.67	−7.24	10.49	0.312
I	38.65	−8.07	10.96	0.316
J	37.44	−5.35	12.89	0.385
K	35.62	−3.20		0.469
L	29.98	−0.69		0.671
M	26.00	−0.33		0.789
N	20.93	−0.71		0.926
O	14.18	−2.06		1.13
P	10.41	−2.97		1.31
Q	7.95	−3.26		1.59
R	5.88	−2.45		2.12
S	4.24	−1.55		2.50
T	1.65	−0.50		2.87
U	3.69	−0.29		2.83
V	0.18	−0.45		0.360
W	3.33	1.87		0.381
X	10.95	7.49		0.343
Y	15.93	11.31	7.81	0.251
Z	19.50	13.87	1.34	0.174

The inverse relationship between the maximum in the reactive delay time and the resonance width, which is demonstrated in Figure 7 for cases of series I and II as well as for several symmetric potentials considered in ref 1, can be illustrated in

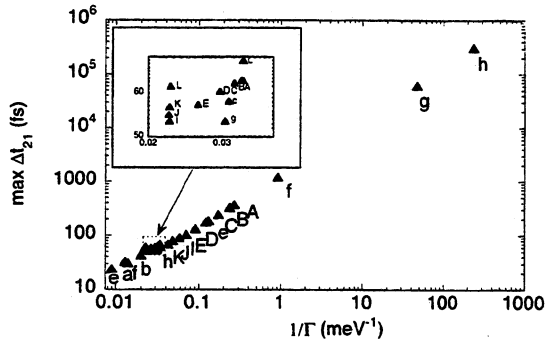

Figure 7. Local maximum in the reactive delay time Δt_{21} curve versus the inverse of the width of the resonance associated with the delay time feature. The cases are labeled as in Table 1. Cases a–c and e–h correspond to calculations of ref 1. The insert in the upper left corner is an expansion of the indicated region.

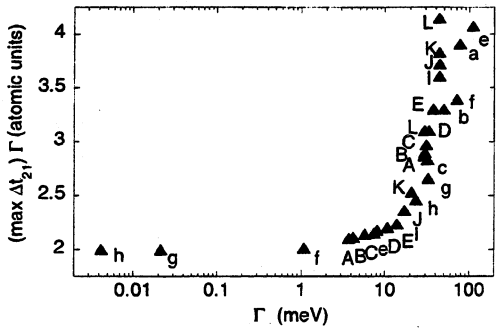

Figure 8. Product of the local maximum in the reactive delay time Δt_{21} curve and the resonance width versus the resonance width. The width is of the resonance that is associated with the delay time feature. The cases are labeled as in Table 1. Cases a–c and e–h correspond to calculations of ref 1.

TABLE 3: Energy E_{max} of the Maximum Delay Time Δt_{21}^{max} and the Resonance Parameters for the Higher Energy Resonance [$E_R(1)$,$\Gamma(1)$] and Lower Energy Resonance [$E_R(2)$,$\Gamma(2)$]

case	E_{max}, meV	Δt_{21}^{max}, fs	$E_R(1)$, meV	$\Gamma(1)$, meV	$E_R(2)$, meV	$\Gamma(2)$, meV
N	244.90	71.27	251.38	44.19	230.45	40.94
O	250.62	76.11	254.38	43.05	240.20	48.47
Q	257.39	80.28	258.01	37.82	250.06	60.16
S	270.85	86.52	270.83	30.98	266.60	77.53
T	284.63	90.81	284.65	28.92	283.00	83.05
U	291.70	92.84	291.64	28.45	287.95	80.60

another way. Although the resonances in this study are, in general, broad, we first consider an isolated narrow resonance (INR), to recall the properties of isolated resonances for comparison. Near an INR, the scattering matrix element S_{ji} can be written as[3]

$$S_{ji}(E) = S_{ji}^0(E) - i\frac{\gamma_j\gamma_i}{E - E_R + i\Gamma/2} \tag{18}$$

where $S_{ji}^0(E)$ is the nonresonant background contribution which is slowly varying with energy and γ_n is the partial width amplitude for channel n. To uncover the limiting behavior of the reactive delay time Δt_{21} at real energies in the vicinity of an INR, let us assume that the partial width amplitudes γ_1 and γ_2 are independent of energy and that S_{12}^0 is independent of energy and is a negligible contributor to $S_{12}(E)$. It is then easily shown analytically that the reactive delay time will have a maximum at $E = E_R$, at which

$$\Delta t_{21} = 2\hbar/\Gamma \tag{19}$$

The relationship $\Delta t_{21}\Gamma = 2\hbar$ is reminiscent of the uncertainty principle, and we might expect that for broader resonances the product of the maximum reactive delay time and the resonance width would exceed $2\hbar$. We have plotted in Figure 8 this product (in units of $\hbar$) versus the resonance width. We have included results from cases of series I, cases of series II for which two peaks in Δt_{21} were observed, and cases a–c and e–h considered in ref 1. As discussed above, and seen in Figures 1–5, there is a very good correspondence between E_R and the energy at which Δt_{21} is a maximum. For cases f–h, the narrow resonances are trapped states lying well below the barrier maximum, and for these resonances we find $\Delta t_{21}\Gamma = 2.0\hbar$, in excellent agreement with eq 19 for an INR. For cases in series I, this product fell between $2.1\hbar$ and $2.3\hbar$ for the lower energy narrower resonances and between $2.8\hbar$ and $3.6\hbar$ for the higher energy broader resonances. For cases J–L, this product fell between $2.3\hbar$ and $3.1\hbar$ for the lower energy narrower resonances and between $3.7\hbar$ and $4.2\hbar$ for the higher energy broader resonances. As the width Γ of the resonance increases, the product generally increases and exceeds $2\hbar$. The above results are in very good agreement with what is expected for narrow and broad resonances.

VI. Concluding Remarks

The structure in the reaction probability for scattering by a one-dimensional potential barrier is associated with poles of the scattering matrix; *i.e.*, increases in the transmission coefficients occur at real energies in the vicinity of the real part of the complex resonance energies. This correlation is further demonstrated by comparing the locations of the maxima in dP_{21}/dE with the values of E_R. The resonances give rise to features not only in the transmission coefficient but also in the reactive delay time. Again, we observe a strong correlation between the locations of maxima in Δt_{21} and values of E_R, as well as a correlation between the maximum in the delay time and the width of the associated resonance.

Since the chemical reaction threshold is responsible for the rise in the reaction probability in the vicinity of the global potential barrier maximum, the present study provides further evidence for the usefulness of treating chemical reaction thresholds as resonances, consistent with our work on model symmetric potential barriers[1] and the paradigm suggested in that work by which the study of chemical reactivity is a study of the poles of the S matrix. These threshold resonances tend to be broader than trapped-state resonances and, therefore, they are associated with smaller delay time peaks.

The present study is also consistent with our work with Chatfield, Schwenke, and Garrett[4,5] on the global control of suprathreshold reactivity in three-dimensional H + H_2 reactions, in which we showed that quantized transition states produce steplike features in the cumulative reaction probability curves for three-dimensional atom–diatom reactions and that these features may be associated with variational transition states. We have interpreted such steps or thresholds as broad resonances. (The cumulative reaction probability (CRP) is analogous to P_{21} in our model studies, and the density of reactive states, which is the energy derivative of the CRP and played a central role in our H + H_2 studies,[4,5] is analogous to $dP_{21}(E)/dE$. The energy derivative, in both the three-dimensional and model studies, helps bring out the discrete structure of the resonances.)

The conclusions reached in the H + H_2 studies have been supported by a number of accurate three-dimensional quantal calculations on other atom–diatom reactive systems, including both H_2X systems (O + H_2,[5,7,25] F + H_2,[26] He + H_2^+,[27] and Ne + H_2^+ [28]) and HX_2 systems (H + O_2,[29] Cl + HCl,[6] I + HI,[6] and I + DI[6]). In these systems the cumulative reaction probability

or a smoothed CRP shows a steplike structure which may represent quantized transition states. Furthermore, many of the steplike features occur at reaction energies which correspond very nicely with maxima in vibrationally adiabatic potential energy curves, consistent with the interpretation of transition-state thresholds as resonances. This interpretation has been utilized in a reformulation of variational transition-state theory using quantum mechanical resonance theory.[23] In addition, Zhao and Rice[30] have recently shown that the identification of transition states as scattering resonances also results from application of a complex scaling transformation to the reaction coordinate of a chemical reaction. Furthermore, their complex scaling analysis also led to a precise definition of the resonance width operator, whose expectation values are resonance lifetimes.

Previous studies[5,7,25] of the asymmetric reaction $O + H_2 \rightarrow OH + H$ may be better understood in light of our model studies presented here. In the previous studies, we have shown that the reaction of O with H_2 is controlled up to high energy by quantized transition states. The transition states correspond to broad resonances whose classical analogues are dynamical bottlenecks which gate reactive flux and which are locally vibrationally adiabatic at threshold energies. There is a correlation between the quantized transition-state threshold energies (obtained via fits to the derivative of the quantum mechanical CRP) and the maxima of semiclassically computed vibrationally adiabatic curves. The latter curves are labeled by the quantum numbers of the stretching (v_1) and bending (v_2) modes of the OH_2 transition state; the stretching motion correlates adiabatically with the vibrational motion of the reactant H_2 and of the product OH. Many of the vibrationally adiabatic curves for this reaction, in particular those with $v_1 \geq 1$, show two potential energy barrier maxima.[7] The barrier in the entrance (reactant approach) valley is larger than that in the product valley; see Figure 1 of ref 7. The quantal calculations[7] have been interpreted to suggest that the transition states occurring at reactantlike geometries in the entrance valley (variational transition states associated with the global maxima in the vibrationally adiabatic curves) exert significant control on $O + H_2$ chemical reactivity. However, some of the transition states occurring at productlike geometries in the exit valley also have important effects on the CRP; we referred to these latter transition states as supernumeraries of the first kind.[7] Other transition states in the exit channel do not appear to influence the overall CRP. Consistent with the above results, we find here that, in the case of unsymmetric one-dimensional potentials having two potential maxima, the quantum mechanical resonance in the vicinity of the global maximum is associated with a rise in the reaction probability toward unity. This resonance is analogous to the variational transition-state threshold. The quantum mechanical resonance in the vicinity of the lower local potential maximum in our model studies sometimes appears to strongly influence the reaction probability (see, *e.g.*, cases B and C), and at other times it appears to have very little if any influence (see, *e.g.*, cases J and K). The former resonances have analogues in the supernumerary transition-state thresholds of the first kind. Although the comparison between the one-dimensional model studies undertaken here and the three-dimensional quantal calculations has definite limitations (since the model studies of single barriers do not consider vibrationally nonadiabatic effects, which may be especially important between multiple barriers, whereas the quantal calculations[7] show significant vibrational nonadiabaticity in the chemical reaction), it is very encouraging that concepts deduced from multidimensional studies can be understood even in part from such simple one-dimensional reaction-path models.

Acknowledgment. We are very grateful to Zhen (Michael) Gu for preparing the figures. R.S.F. acknowledges useful conversations with Professor Ronald Duchovic. This work was supported by the donors of The Petroleum Research Fund, administered by the Americal Chemical Society, by a Purdue Research Foundation Summer Faculty Grant, by an Indiana University Purdue University Fort Wayne Summer Faculty Research Grant, and by a grant from the U.S. Department of Energy, Office of Basic Energy Sciences. Computational resources were provided by the Chemistry Department at IPFW, and graphics resources were provided by Minnesota Supercomputer Institute.

References and Notes

(1) Friedman, R. S.; Truhlar, D. G. *Chem. Phys. Lett.* **1991**, *183*, 539.
(2) Siegert, A. J. F. *Phys. Rev.* **1939**, *56*, 750.
(3) Taylor, J. R. *Scattering Theory*; Wiley: New York, 1972.
(4) (a) Chatfield, D. C.; Friedman, R. S.; Truhlar, D. G.; Garrett, B. C.; Schwenke, D. W. *J. Am. Chem. Soc.* **1991**, *113*, 486. (b) Chatfield, D. C.; Friedman, R. S.; Truhlar, D. G.; Schwenke, D. W. *Faraday Discuss. Chem. Soc.* **1991**, *91*, 289.
(5) Chatfield, D. C.; Friedman, R. S.; Schwenke, D. W.; Truhlar, D. G. *J. Phys. Chem.* **1992**, *96*, 2414.
(6) Chatfield, D. C.; Friedman, R. S.; Lynch, G. C.; Truhlar, D. G. *J. Phys. Chem.* **1992**, *96*, 57. The cumulative reaction probabilities were presented in: (a) Schatz, G. C. *J. Chem. Phys.* **1989**, *90*, 3582. (b) Schatz, G. C. *J. Chem. Phys.* **1989**, *90*, 4847. (c) Schatz, G. C. *J. Chem. Soc. Faraday Trans.* **1990**, *86*, 1729.
(7) Chatfield, D. C.; Friedman, R. S.; Lynch, G. C.; Truhlar, D. G.; Schwenke, D. W. *J. Chem. Phys.* **1993**, *98*, 342.
(8) Messiah, A. *Quantum Mechanics*; Wiley: New York, 1966; pp 85ff, 92.
(9) Basilevsky, M. V.; Ryaboy, V. M. *Int. J. Quantum Chem.* **1981**, *19*, 611.
(10) Smith, F. T. *Phys. Rev.* **1960**, *118*, 349.
(11) International Mathematical and Statistical Library, Version 2.0, IMSL Inc., Houston, Sept 1991.
(12) Gear, C. W. *Numerical Initial Value Problems in Ordinary Differential Equations*; Prentice-Hall: Englewood Cliffs, NJ, 1971.
(13) Bellman, R.; Kalaba, R.; Prestrud, M. *Invariant Imbedding and Radiative Transfer in Slabs of Finite Thickness*; American Elsevier: New York, 1963.
(14) Riley, M. E. Ph.D. Thesis, California Institute of Technology, Pasadena, CA, 1968.
(15) Press, W. H.; Flannery, B. P.; Teukolsky, S. A.; Vetterling, W. T. *Numerical Recipes*; Cambridge Univ. Press: Cambridge, 1986.
(16) Zhao, M.; Mladenovic, M.; Truhlar, D. G.; Schwenke, D. W.; Sharafeddin, O.; Sun, Y.; Kouri, D. J. *J. Chem. Phys.* **1989**, *91*, 5302.
(17) Garrett, B. C.; Truhlar, D. G. *Int. J. Quantum. Chem.* **1986**, *29*, 1463.
(18) Mandelshtam, V. A.; Taylor, H. S. *J. Chem. Phys.* **1993**, *99*, 222.
(19) Ryaboy, V.; Lefebvre, R. *J. Chem. Phys.* **1993**, *99*, 9547.
(20) Atabek, O.; Lefebvre, R.; Garcia Sucre, M.; Gomez-Llorente, J.; Taylor, H. *Int. J. Quant. Chem.* **1991**, *40*, 211.
(21) Seideman, T.; Miller, W. H. *J. Chem. Phys.* **1991**, *95*, 1768.
(22) Ryaboy, V.; Moiseyev, N. *J. Chem. Phys.* **1993**, *98*, 9618.
(23) Truhlar, D. G.; Garrett, B. C. *J. Phys. Chem.* **1992**, *96*, 6515.
(24) (a) Zewail, A. H.; Bernstein, R. B. *Chem. Eng. News* **Nov. 7, 1988**, *66*, 24. (b) Khundkar, L. R.; Zewail, A. H. *Annu. Rev. Phys. Chem.* **1990**, *41*, 15. (c) Zewail, A. H. *Faraday Discuss. Chem. Soc.* **1991** *91*, 207. (d) Zewail, A. H. *J. Phys. Chem.* **1993**, *97*, 12427. (e) Materny, A.; Herek, J. L.; Cong, P.; Zewail, A. H. *J. Phys. Chem.* **1994**, *98*, 3352.
(25) (a) Haug, K.; Schwenke, D. W.; Truhlar, D. G.; Zhang, Y.; Zhang, J. Z. H.; Kouri, D. J. *J. Chem. Phys.* **1987**, *87*, 1892. (b) Bowman, J. M. *Chem. Phys. Lett.* **1987**, *141*, 545. (c) Bowman, J. M. *Faraday Discuss. Chem. Soc.* **1991**, *91*, 385. (d) Truhlar, D. G. *Faraday Discuss. Chem. Soc.* **1991**, *91*, 395.
(26) (a) Lynch, G. C.; Halvick, P.; Zhao, M.; Truhlar, D. G.; Yu, C.-h.; Kouri, D. J.; Schwenke, D. W. *J. Chem. Phys.* **1991**, *94*, 7150. (b) Kress, J. D.; Hayes, E. F. *J. Chem. Phys.* **1992**, *97*, 4881 and references therein.
(27) (a) Darakjian, Z.; Hayes, E. F.; Parker, G. A.; Butcher, E. A.; Kress, J. D. *J. Chem. Phys.* **1991**, *95*, 2516. (b) Klippenstein, S. J.; Kress, J. D. *J. Chem. Phys.* **1992**, *96*, 8164.
(28) (a) Kress, J. D. *J. Chem. Phys.* **1991**, *95*, 8673. (b) Kress, J. D.; Klippenstein, S. J. *Chem. Phys. Lett.* **1992**, *195*, 513. (c) Kress, J. D.; Walker, R. B.; Hayes, E. F.; Pendergast, P. *J. Chem. Phys.* **1994**, *100*, 2728.
(29) (a) Pack, R. T.; Butcher, E. A.; Parker, G. A. *J. Chem. Phys.* **1993**, *11*, 9310. (b) Leforestier, C.; Miller, W. H. *J. Chem. Phys.* **1994**, *100*, 733.
(30) Zhao, M.; Rice, S. A. *J. Phys. Chem.* **1994**, *98*, 3444.

JP9421848